УЧЕНЫЕ ЗАПИСКИ КАЗАНСКОГО ГОСУДАРСТВЕННОГО УНИВЕРСИТЕТА
Том 148, кн. 3 Физико-математические науки *2006*

UDK 517.958:57+519.63

NUMERICAL MODELING OF THE DESIGN OF BIFURCATED PROSTHESES USED IN THE TREATMENT OF ABDOMINAL AORTIC ANEURYSM

S. Lapin, S. Čanić

Abstract

The main goal of this paper is to address the numerical solution of the problem of fluid-structure interaction between blood and arterial walls. We use one-dimensional effective model derived asymptotically from the Navier – Stokes equations describing blood flow and the linear elastic membrane equation for arterial walls. In this study we consider case with bifurcated compliant arteries with inserted prosthesis. We use the derived model to estimate the influence of a shear stress on the developing of atherogenesis.

1. Introduction

1.1. Background of the problem. The dynamic interaction between a fluid and a structure is a mechanism that is seen in many different physical phenomena. One of the fluid structure interaction problems receiving a lot of attention in recent years is the problem arising in hemodynamics applications. In this paper we consider numerical simulation of the blood flow through branching arteries with an inserted prostheses called stents and stent-grafts [1]. Both the arteries and the stents are assumed to be elastic. The Young's modulus of elasticity for arteries was obtained from [2]. The Young's modulus of elasticity of stents was obtained from the measurements by K. Ravi-Chandar and R. Wang [3, 4]. The underlying problem consists of modeling the flow through the human aorta branching into iliac arteries, that suffers from an *aortic abdominal aneurysm* (AAA).

Non-surgical treatment of AAA consists of inserting a prosthesis inside the diseased aorta to redirect the flow of blood and lower the pressure to the aneurysmal walls. There are various complications associated with this procedure, they include stent-graft migration, occlusion of the graft limbs and formation of new aneurysms near the anchoring sites [5]. The purpose of the study presented here is to use mathematical modeling and numerical simulations to understand some of the hemodynamic factors that might be responsible for the complications listed above, and suggest an improved prosthesis design that might minimize some of the problems.

1.2. Mathematical model. We use a reduced, one dimensional model, together with the special conditions derived via Riemann invariants, to simulate the flow through the branching arteries. The model is derived using an asymptotic reduction of the Navier – Stokes equations modeling blood with the linear elastic membrane equation for the wall.

The resulting set of equations is used to study the optimal prostheses design by investigating the impact of shear stress rates on the initiation of focal atherogenesis.

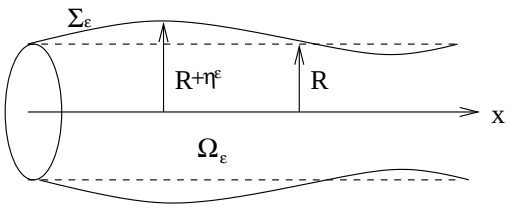

Fig. 1. Computational domain

2. Effective model derivation

We consider the unsteady axisymmetric flow of a Newtonian incompressible fluid in a thin elastic cylinder whose radius is small with respect to its length. We define the ratio $\varepsilon = R/L$, where R is the radius and L is the length of the cylinder. Now, for every fixed $\varepsilon > 0$ we introduce the computational domain (Figure 1)

$$\Omega_\varepsilon(t) = \{x \in \mathbb{R}^3; \quad x = (r\cos\Theta, r\sin\Theta, x), \quad r < R + \eta^\varepsilon(x,t), \quad 0 < x < L\},$$

where $\eta^\varepsilon(x,t)$ is the radial wall displacement.

This domain is filled with fluid modeled by the incompressible Navier−Stokes equations. We assume that the flow is axially symmetric, so the fluid velocity is $\mathbf{v}^\varepsilon(r,x,t) = (v_r^\varepsilon(r,x,t), v_x^\varepsilon(r,x,t))$; the pressure defined by $p^\varepsilon(r,x,t) - p_{\text{ref}}$ with p_{ref} being constant reference pressure.

Now the problem in an Eulerian framework in cylindrical coordinates in $\Omega_\varepsilon(t) \times \mathbb{R}_+$ reads as follows

$$\rho\left[\frac{\partial v_r^\varepsilon}{\partial t} + v_r^\varepsilon\frac{\partial v_r^\varepsilon}{\partial r} + v_x^\varepsilon\frac{\partial v_r^\varepsilon}{\partial x}\right] - \mu\left[\frac{\partial^2 v_r^\varepsilon}{\partial r^2} + \frac{1}{r}\frac{\partial v_r^\varepsilon}{\partial r} + \frac{\partial^2 v_r^\varepsilon}{\partial x^2} - \frac{v_r^\varepsilon}{r^2}\right] + \frac{\partial p^\varepsilon}{\partial r} = 0, \tag{1}$$

$$\rho\left[\frac{\partial v_x^\varepsilon}{\partial t} + v_r^\varepsilon\frac{\partial v_x^\varepsilon}{\partial r} + v_x^\varepsilon\frac{\partial v_x^\varepsilon}{\partial x}\right] - \mu\left[\frac{\partial^2 v_x^\varepsilon}{\partial r^2} + \frac{1}{r}\frac{\partial v_x^\varepsilon}{\partial r} + \frac{\partial^2 v_x^\varepsilon}{\partial x^2}\right] + \frac{\partial p^\varepsilon}{\partial x} = 0, \tag{2}$$

$$\frac{\partial v_r^\varepsilon}{\partial r} + \frac{\partial v_x^\varepsilon}{\partial x} + \frac{v_r^\varepsilon}{r} = 0, \tag{3}$$

where μ is the fluid dynamic viscosity, and ρ is the fluid density.

Further we assume that the lateral wall of the cylinder $\Sigma_\varepsilon(t) = \{r = R + \eta^\varepsilon(x,t)\} \times$ $\times(0,L)$ is elastic and allows only radial displacement. We can describe its motion (in Lagrangian coordinates) using the linear elastic membrane equation.

The radial contact force is given by [6]

$$F_r = -\frac{h(\varepsilon)E(\varepsilon)}{1-\sigma^2}\frac{\eta^\varepsilon}{R^2} - p_{\text{ref}}\frac{\eta}{R} - \rho_w h(\varepsilon)\frac{\partial^2\eta^\varepsilon}{\partial t^2}, \tag{4}$$

where F_r is the radial component of external forces (coming from the stresses induced by the fluid), $h = h(\varepsilon)$ is the membrane thickness, ρ_w is the wall volumetric mass, $E = E(\varepsilon)$ is the Young's modulus, $0 < \sigma \leq 0.5$ is the Poisson ratio. Typical values of the parameters are given in Table 1.

The fluid equations are coupled with the membrane equation through the lateral boundary conditions requiring the continuity of velocity and balance of forces. Now we consider the balance of forces, namely we set the radial contact force equal to the radial component of the force exerted by the fluid.

The fluid contact force is given in Eulerian coordinates as

$$F_f = ((p^\varepsilon - p_{\text{ref}})I - 2\mu D(v^\varepsilon))ne_r,$$

Table 1. Parameter values

Parameters	Values
ε	$0.002 - 0.06$
Characteristic radius: R_0	$0.0025 - 0.012$ m
Characteristic length: L	$0.065 - 0.2$ m
Young's modulus: E	$10^5 - 10^6$ Pa [2]
Wall thickness: h	$1 - 2 \times 10^{-3}$ m
Blood density: ρ	1050 kg/m^3
Reference pressure: p_{ref}	13000 Pa = 97.5 mmHg

where $D(v^\varepsilon)$ is the symmetrized gradient of velocity defined by,

$$D(v^\varepsilon) = \frac{1}{2}(\nabla v^\varepsilon + (\nabla v^\varepsilon)^t).$$

Using the Jacobian of the transformation from Eulerian to Lagrangian coordinates we have (pointwise):

$$-F_r = ((p^\varepsilon - p_{\text{ref}})I - 2\mu D(v^\varepsilon))ne_r(1 + \frac{\eta^\varepsilon}{R})\sqrt{1 + (\frac{\partial \eta^\varepsilon}{\partial x})^2} \quad \text{on} \quad \Sigma_\varepsilon^0 \times \mathbb{R}_+. \tag{5}$$

The initial data are given by,

$$\eta^\varepsilon = \frac{\partial \eta^\varepsilon}{\partial t} = 0 \ \text{ and } \ v^\varepsilon = 0 \quad \text{on} \ \ \Sigma_\varepsilon(0) \times \{0\}. \tag{6}$$

We assume that the end-points of the tube are fixed and that the problem is driven by a time-dependent pressure drop between the inlet and outlet boundary. Therefore, we have the following inlet-outlet boundary conditions:

$$v_r^\varepsilon = 0, \quad p^\varepsilon + \rho(v_x^\varepsilon)^2/2 = P_1(t) + p_{\text{ref}} \quad \text{on} \quad (\partial\Omega_\varepsilon(t) \cap \{x = 0\}) \times \mathbb{R}_+, \tag{7}$$

$$v_r^\varepsilon = 0, \quad p^\varepsilon + \rho(v_x^\varepsilon)^2/2 = P_2(t) + p_{\text{ref}} \quad \text{on} \ \ (\partial\Omega_\varepsilon(t) \cap \{x = L\}) \times \mathbb{R}_+, \tag{8}$$

$$\eta^\varepsilon = 0 \ \text{ for } \ x = 0, \quad \eta^\varepsilon = 0 \ \text{ for } \ x = L \ \text{ and } \ \forall t \in \mathbb{R}_+. \tag{9}$$

We will assume that the pressure drop, $A(t) = P_1(t) - P_2(t) \in C_0^\infty(0, +\infty)$.

2.1. Asymptotic reduction of the model. Now, using the asymptotic techniques described in detail in [7, 8] we will obtain the reduced, two-dimensional equations.

In order to represent the equations (1)–(3) in nondimensional form we introduce the independent variables $\tilde{r}$, $\tilde{x}$ and $\tilde{t}$

- $r = R\tilde{r}$,
- $x = L\tilde{x}$,
- $t = \dfrac{1}{\omega^\varepsilon}\tilde{t}$, where $\omega^\varepsilon = \dfrac{1}{L}\sqrt{\dfrac{hE}{R\rho(1-\sigma^2)}}$.

Further, we introduce the following asymptotic expansions

$$v^\varepsilon = V\{\tilde{v}^0 + \varepsilon\tilde{v}^1 + \cdots\}, \quad \text{with } V = \sqrt{\frac{R(1-\sigma^2)}{\rho h E}}\mathcal{P}, \tag{10}$$

$$\eta^\varepsilon = \Xi\{\tilde{\eta}^0 + \varepsilon\tilde{\eta}^1 + \cdots\}, \quad \text{with } \Xi = \frac{R^2(1-\sigma^2)}{hE}\mathcal{P}, \tag{11}$$

$$p^\varepsilon = \rho V^2\{\tilde{p}^0 + \varepsilon\tilde{p}^1 + \cdots\}. \tag{12}$$

Here $\mathcal{P}$ denotes a norm that measures the magnitude of inlet and outlet pressure, the pressure drop, and the averaged pressure in one cardiac cycle [7].

After ignoring the terms of order ε^2 and smaller the momentum equations and the incompressibility condition become

$$\mathrm{Sh}\frac{\partial\tilde{v}_x^\varepsilon}{\partial t} + \tilde{v}_x^\varepsilon\frac{\partial\tilde{v}_x^\varepsilon}{\partial\tilde{x}} + \tilde{v}_r^\varepsilon\frac{\partial\tilde{v}_x^\varepsilon}{\partial\tilde{r}} - \frac{1}{\mathrm{Re}}\left[\frac{1}{\tilde{r}}\frac{\partial}{\partial\tilde{r}}\left(\tilde{r}\frac{\partial v_z^\varepsilon}{\partial\tilde{r}}\right)\right] = 0, \tag{13}$$

$$\frac{\partial\tilde{p}}{\partial\tilde{r}} = 0, \tag{14}$$

$$\frac{\partial}{\partial\tilde{r}}(\tilde{r}\tilde{v}_r) + \frac{\partial}{\partial\tilde{x}}(\tilde{r}\tilde{v}_x) = 0, \tag{15}$$

where $\mathrm{Sh} = (L\omega^\varepsilon)/V$ and $\mathrm{Re} = (\rho V R^2)/(\mu L)$.

The leading order linear elastic membrane equation read

$$-F_r = \mathcal{P}\tilde{\eta} + O(\varepsilon^2). \tag{16}$$

The asymptotic form of the contact force derived from (5) becomes

$$((p^\varepsilon - p_{\mathrm{ref}})I - 2\mu D(v^\varepsilon))ne_r = \rho V^2(p^\varepsilon - p_{\mathrm{ref}} + O(\varepsilon^2))\left(1 + \frac{\Xi}{R}\tilde{\eta}\right).$$

Therefore, we obtain the following leading order relationship between the pressure and the radial displacement

$$(\tilde{p}^\varepsilon - \tilde{p}_{\mathrm{ref}}) = \frac{\mathcal{P}}{\rho V^2}\cdot\frac{\tilde{\eta}}{1+\frac{\Xi}{R}\tilde{\eta}} = \frac{\mathcal{P}}{\rho V^2\Xi}\frac{\Xi}{R}\tilde{\eta}\left(1 - \frac{\Xi}{R}\tilde{\eta} + ...\right) =$$

$$= \frac{\mathcal{P}R}{\rho V^2\Xi}\left(\frac{\Xi}{R}\tilde{\eta} - \left(\frac{\Xi}{R}\tilde{\eta}\right)^2\cdots\right). \tag{17}$$

We assume that Ξ/R is of order ε so the last term on right-hand side of (17) can be ignored and we obtain

$$\tilde{p}^\varepsilon - \tilde{p}_{\mathrm{ref}} = \frac{\mathcal{P}R}{\rho V^2}\tilde{\eta}, \tag{18}$$

which in dimensional variables gives us the Law of Laplace,

$$p^\varepsilon - p_{\mathrm{ref}} = \frac{Eh}{(1-\sigma^2)R}\,\frac{\eta}{R}. \tag{19}$$

Having the above results in hand, we proceed by introducing the reduced two-dimensional model written in non-dimensional variables.

We define the scaled domain

$$\tilde{\Omega}(\tilde{t}) = \left\{(\tilde{x},\tilde{r}) \in \mathbb{R}^2 | \tilde{r} < 1 + \frac{\Xi}{R}\eta(\tilde{x},\tilde{t}), \quad 0 < \tilde{x} < 1\right\},$$

and the lateral boundary $\tilde{\Sigma}(\tilde{t}) = \{\tilde{r} = 1 + \frac{\Xi}{R}\eta(\tilde{x},\tilde{t})\} \times (0,1)$.

Now we formulate the two-dimensional problem in the following way,
Find a triple $(\tilde{v}_x, \tilde{v}_r, \tilde{\eta})$ *satisfying*

$$\mathrm{Sh}\frac{\partial \tilde{v}_x^\varepsilon}{\partial \tilde{t}} + \tilde{v}_x^\varepsilon \frac{\partial \tilde{v}_x^\varepsilon}{\partial \tilde{x}} + \tilde{v}_r^\varepsilon \frac{\partial \tilde{v}_x^\varepsilon}{\partial \tilde{r}} + \frac{\partial \tilde{p}}{\partial \tilde{x}} = \frac{1}{\mathrm{Re}}\left[\frac{1}{\tilde{r}}\frac{\partial}{\partial \tilde{r}}\left(\tilde{r}\frac{\partial v_z^\varepsilon}{\partial \tilde{r}}\right)\right], \tag{20}$$

$$\frac{\partial}{\partial \tilde{r}}(\tilde{r}\tilde{v}_r) + \frac{\partial}{\partial \tilde{x}}(\tilde{r}\tilde{v}_x) = 0, \tag{21}$$

$$(\tilde{p}^\varepsilon - \tilde{p}_{\mathrm{ref}}) = \frac{\mathcal{P}R}{\rho V^2}\tilde{\eta}, \tag{22}$$

$$\tilde{v}_r(\tilde{x}, 1 + \frac{\Xi}{R}\tilde{\eta}(x,t), \tilde{t}) = \frac{\partial \tilde{\eta}}{\partial \tilde{t}},\ \tilde{v}_x = 0, \tag{23}$$

with the initial and boundary conditions given by

$$\tilde{\eta} = \frac{\partial \tilde{\eta}}{\partial \tilde{t}} = 0 \quad \text{at} \quad \tilde{t} = 0, \tag{24}$$

$$\tilde{v}_r^\varepsilon = 0, \quad \tilde{p} = (P_1(\tilde{t}) + p_{\mathrm{ref}})/(\rho V^2) \quad \text{on} \quad (\partial\Omega_\varepsilon(t) \cap \{\tilde{x} = 0\}) \times \mathbb{R}_+, \tag{25}$$

$$\tilde{v}_r^\varepsilon = 0, \quad \tilde{p} = (P_2(\tilde{t}) + p_{\mathrm{ref}})/(\rho V^2) \quad \text{on} \quad (\partial\Omega_\varepsilon(t) \cap \{\tilde{x} = 1\}) \times \mathbb{R}_+, \tag{26}$$

$$\tilde{\eta} = 0 \ \text{ for } \ \tilde{x} = 0, \quad \tilde{\eta} = 0 \ \text{ for } \ \tilde{x} = 1 \ \text{ and } \ \forall \tilde{t} \in \mathbb{R}_+. \tag{27}$$

The model defined above is a free-boundary degenerate hyperbolic system with parabolic regularization. This system, though already simplified, is still quite complex. The theoretical analysis and numerical simulation of (20)–(27) is a difficult task; that is why we will proceed further in order to obtain a simplified one-dimensional reduced model.

2.2. Derivation of the one-dimensional reduced model. In order to derive a simplified one-dimensional model we express the two-dimensional equations in terms of the averaged quantities across the cross-sectional area.

Let us introduce $\tilde{A} = (1 + \frac{\Xi}{R}\tilde{\eta})^2$ and $\tilde{m} = \tilde{A}\tilde{U}$ where

$$\tilde{U} = \frac{2}{\tilde{A}} \int_0^{1+\frac{\Xi}{R}\tilde{\eta}} \tilde{v_x}\tilde{r}d\tilde{r}, \tag{28}$$

$$\tilde{\alpha} = \frac{2}{\tilde{A}\tilde{U}^2} \int_0^{1+\frac{\Xi}{R}\tilde{\eta}} 2\tilde{v_x}^2\tilde{r}d\tilde{r}. \tag{29}$$

Now we integrate the equations (20)–(21) from $\tilde{r} = 0$ to $\tilde{r} = 1 + \frac{\Xi}{R}\tilde{\eta}$ and then express them in terms of the averaged quantities. Using the no-slip condition at the lateral boundary we obtain

$$\begin{gathered}\frac{\partial \tilde{A}}{\partial \tilde{t}} + \frac{\Xi}{R}\frac{\partial \tilde{m}}{\partial \tilde{x}} = 0,\\ \mathrm{Sh}\frac{\partial \tilde{m}}{\partial \tilde{t}} + \frac{\partial}{\partial \tilde{x}}\left(\frac{\tilde{\alpha}\tilde{m}^2}{\tilde{A}}\right) + \tilde{A}\frac{\partial \tilde{p}}{\partial \tilde{x}} = \frac{2}{\mathrm{Re}}\sqrt{\tilde{A}}\left[\frac{\partial \tilde{v}_x}{\partial \tilde{r}}\right]_{\tilde{\Sigma}}.\end{gathered} \tag{30}$$

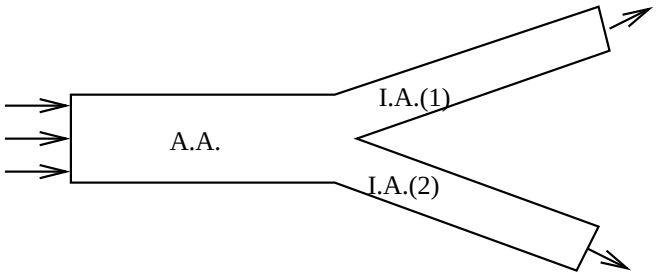

Fig. 2. Blood flow through abdominal aorta (A.A) and iliac arteries (I.A.(1) and I.A.(2))

The next step is to specify the axial velocity profile $\tilde{v}_x$ in terms of the averaged quantities. The typical approximation (corresponding to Poiseuille flow [9]) is

$$\tilde{v}_x = \frac{\gamma+2}{\gamma}\tilde{U}\left[1-\left(\frac{\tilde{r}}{1+\frac{\Xi}{R}\tilde{\eta}}\right)^{\gamma}\right]. \tag{31}$$

We assume that $\gamma = 9$, which corresponds to the non-Newtonian flow of blood [10, 11].

After plugging (31) into (27) the right hand side becomes

$$\frac{-2(\gamma+2)}{\mathrm{Re}}\frac{\tilde{m}}{\tilde{A}}.$$

Using A_0 to denote the non-stressed area R^2 we obtain a one-dimensional system written in dimensional variables

$$\frac{\partial A}{\partial t}+\frac{\partial m}{\partial x}=0, \tag{32}$$

$$\frac{\partial m}{\partial t}+\frac{\partial}{\partial x}\left(\frac{\alpha m^2}{A}\right)+\frac{A}{\rho}\frac{\partial p}{\partial x}=-\frac{2\mu}{\rho}(\gamma+2)\frac{m}{A}, \tag{33}$$

$$p := p-p_{\mathrm{ref}}=\left(\frac{Eh}{(1-\sigma^2)R}\left(\sqrt{\frac{A}{A_0}}-1\right)\right). \tag{34}$$

We use $\sigma = 0.5$, so equation (34) reduces to

$$p = G_0\left(\sqrt{\frac{A}{A_0}}-1\right), \tag{35}$$

with $G_0 = (4Eh)/(3R)$.

3. Conditions at the bifurcation point

We use the system of equations (32)–(33) and (35) to model blood flow through the abdominal aorta branching into the iliac arteries (Fig. 2).

One of the important questions here is how to model the flow at the branching point. We use the continuity of pressure and conservation of mass condition to couple the flow exiting the abdominal aorta with the flow entering the iliac arteries [12]. It was shown in [13] that the 1-D approximation to the flow at the branching point for the

fixed geometry provides $\varepsilon^{1/2}$ accuracy to the 3-D flow for small to moderate Reynolds numbers.

We calculate the continuity of pressure and conservation of mass condition at the branching point using the concept of Riemann invariants for a hyperbolic system. More precisely, let us write the system (32)–(33) and (35) in quasilinear form:

$$\begin{pmatrix} A_t \\ m_t \end{pmatrix} + \begin{pmatrix} 0 & 1 \\ -\dfrac{m^2}{A^2} + \dfrac{1}{\rho} A p'(A) & \dfrac{2m}{A} \end{pmatrix} \begin{pmatrix} A_x \\ m_x \end{pmatrix} = \begin{pmatrix} 0 \\ -2\dfrac{\alpha}{\alpha - 1} \nu \frac{m}{A} \end{pmatrix} \tag{36}$$

The eigenvalues of (36) are

$$\lambda_1 = \frac{m}{A} - \sqrt{\frac{1}{2}\frac{G_0}{\rho}\left(\frac{A}{A_0}\right)^{1/2}}, \quad \lambda_2 = \frac{m}{A} + \sqrt{\frac{1}{2}\frac{G_0}{\rho}\left(\frac{A}{A_0}\right)^{1/2}}. \tag{37}$$

Let us further use the following notation:

$$\tilde{c} = \sqrt{\frac{1}{2}\frac{G_0}{\rho} A_0^{-1/2}}.$$

One can show that the right eigenvectors corresponding to λ_1 and λ_2 are given by

$$r_1 = \begin{pmatrix} 1 \\ \lambda_1 \end{pmatrix}, \quad r_2 = \begin{pmatrix} 1 \\ \lambda_2 \end{pmatrix}. \tag{38}$$

Consider Riemann invariants w and z corresponding to the eigenvalues λ_1 and λ_2 respectively. Then w and z satisfy the following equations [14]:

$$\nabla w \cdot r_{\lambda_1} = 0, \quad \nabla z \cdot r_{\lambda_2} = 0, \tag{39}$$

Direct calculations give us

$$w = \frac{m}{A} + 4\sqrt{\frac{1}{2}\frac{G_0}{\rho}\left(\frac{A}{A_0}\right)^{1/2}}, \tag{40}$$

$$z = \frac{m}{A} - 4\sqrt{\frac{1}{2}\frac{G_0}{\rho}\left(\frac{A}{A_0}\right)^{1/2}}. \tag{41}$$

Now, we assume that the bifurcation occurs at a point and that there is no leakage at the bifurcation. Then the outflow from the abdominal aorta ("parent" vessel) should be balanced by the inflow into the iliac arteries ("daughter" vessels) [12]:

$$m_p = m_{d1} + m_{d2}, \tag{42}$$

which describes conservation of mass. We also assume the continuity of pressure

$$p_p = p_{d1} = p_{d2}, \tag{43}$$

here subscript p corresponds to the "parent"vessel and $d1$, $d2$ correspond to the "daughter" vessels.

The Riemann invariants for the "parent" and the two "daughter" vessels read as follows:

$$w_p = \frac{m_p}{A_p} + \tilde{c}_p 4 A_p^{1/4}, \tag{44}$$

$$z_{d1} = \frac{m_{d1}}{A_{d1}} - \tilde{c}_{d1} 4 A_{d1}^{1/4}, \tag{45}$$

$$z_{d2} = \frac{m_{d2}}{A_{d2}} - \tilde{c}_{d2} 4 A_{d2}^{1/4}. \tag{46}$$

From the equations (35) and (42)–(46) it is straightforward to obtain

$$A_p^{1/4} = \frac{w_p - \dfrac{A_{0d1}}{A_{0p}} z_{d1} - \dfrac{A_{0d2}}{A_{0p}} z_{d2}}{4\left(\tilde{c}_p + \tilde{c}_{d1}\left(\dfrac{A_{0d1}}{A_{0p}}\right)^{5/4} + \tilde{c}_{d2}\left(\dfrac{A_{0d2}}{A_{0p}}\right)^{5/4}\right)}. \tag{47}$$

Thus, using Riemann invariants and conditions (42) and (43) we can calculate A_p, A_{d1}, m_p, m_{d1} and m_{d2} in terms of the Riemann invariants w_p, z_{d1} and z_{d2}. The "forward" Riemann invariant w_p and the "backward" Riemann invariants z_{d1} and z_{d2} are known from the initial conditions and the inlet and outlet boundary data.

4. Numerical method

In order to solve equations (32)–(33) and (35) we rewrite them first in conservation form. We take into account that A_0 can depend on x and write the equations in conservation form as follows

$$\frac{\partial}{\partial t} U + \frac{\partial}{\partial x} F = S, \tag{48}$$

where

$$U = \begin{bmatrix} A \\ m \end{bmatrix}, \qquad F(U) = \begin{bmatrix} m \\ \dfrac{\alpha m^2}{A} + \dfrac{G_0}{3\rho}\left(\dfrac{A}{A_0}\right)^{3/2} A_0 \end{bmatrix}, \tag{49}$$

and

$$S(U) = \begin{bmatrix} 0 \\ -2\dfrac{\alpha}{\alpha - 1}\dfrac{m}{A} + \dfrac{G_0}{3\rho}\left(\dfrac{A}{A_0}\right)^{3/2} A_0' \end{bmatrix}. \tag{50}$$

For the numerical solution of the problem stated above we apply the two-step Lax–Wendroff method [15]. We assume here that the grid is uniform, with Δx denoting the mesh step size and Δt the time step, then we define U_m^n to be the approximation of the solution at $(m\Delta x, n\Delta t)$. The method takes the following form

$$U_m^{n+1} = U_m^n - \frac{\Delta t}{\Delta x}\left(F(U_{m+1/2}^{n+1/2}) - F(U_{m-1/2}^{n+1/2})\right) + \frac{\Delta t}{2}\left(S(U_{m+1/2}^{n+1/2}) + S(U_{m-1/2}^{n+1/2})\right),$$

where

$$U_j^{n+1/2} = \frac{U_{j+1/2}^n + U_{j-1/2}^n}{2} + \\ + \frac{\Delta t}{2}\left(-\frac{F(U_{j+1/2}^n) - F(U_{j-1/2}^n)}{\Delta x} + \frac{S(U_{j+1/2}^n) + S(U_{j-1/2}^n)}{2}\right)$$

for $j = m + 1/2$ and $j = m - 1/2$.

The method is stable if the CFL condition

$$\max|\lambda_1, \lambda_2|\frac{\Delta t}{\Delta x} = \max\left|\frac{\alpha m}{A} \pm \sqrt{\alpha(\alpha - 1)\left(\frac{m}{A}\right)^2 + \frac{G_0}{2\rho}\left(\frac{A}{A_0}\right)^{1/2}}\right| \frac{\Delta t}{\Delta x} < 1,$$

is satisfied.

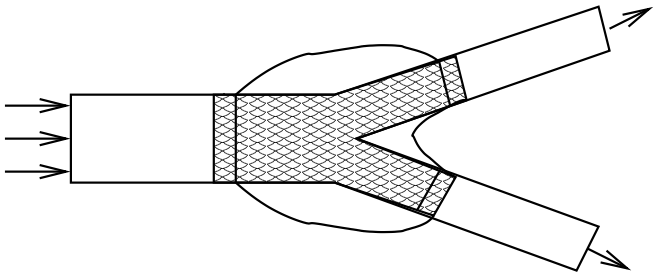

Fig. 3. Aneurysmal abdominal aorta and iliac arteries with inserted bifurcated stent

5. Numerical experiments

We use the numerical method described above to study blood flow through the aneurysmal prostheses (see Fig. 3). We considered two kinds of prostheses:

- Fabric covered "rigid" stent-grafts, such as AneuRx $^{\text{TM}}$.
- Highly compliant bare stents, such as `Wallstent`.

The goal of this study was to understand the influence of the elastic properties of the prosthesis on the stresses exerted by the prostheses to the walls of the native aorta. In particular we were interested in understanding what hemodynamic factors are related to the occlusion of graft limbs, observed in patients and reported in [5, 16].

Many researchers have shown that the wall shear stress has a significant influence on blood coagulation and thrombosis, endothelial cell structure and function.

C.K. Zarins *et al.*([17, 18]) proposed a method called Oscillatory Shear Index (OSI) to quantify the degree of oscillation in shear direction. OSI can be calculated using the following formula:

$$\text{OSI} = \frac{|A_{\text{neg}}|}{|A_{\text{pos}}| + |A_{\text{neg}}|},$$

where A_{neg} and A_{pos} are the areas under the shear stress vs. time when the shear stress is negative and positive respectively.

M. Haidekker, C. White and J.A. Frangos suggested that the spatial and temporal gradients of the shear stress must be separated in order to identify which one is the primary cause of atherosclerotic plaque. In their paper [19], they presented a study implicating high shear stress rate (or the temporal gradient of shear stress) as the main hemodynamic factor responsible for the initiation of focal atherogenesis.

We studied the Oscillatory Shear Index and the shear stress rate to detect possible causes for graft limb occlusion.

The following two parameters were varied in our study:

- prostheses flexibility (Young's modulus),
- prostheses diameter.

We have used the following data in our computations:

- Young's modulus $E_c = 8700$ Pa and $E_r = 217500$ Pa for compliant and rigid stents respectively
- Young's modulus of a human aorta $E_a = 10^5$ Pa

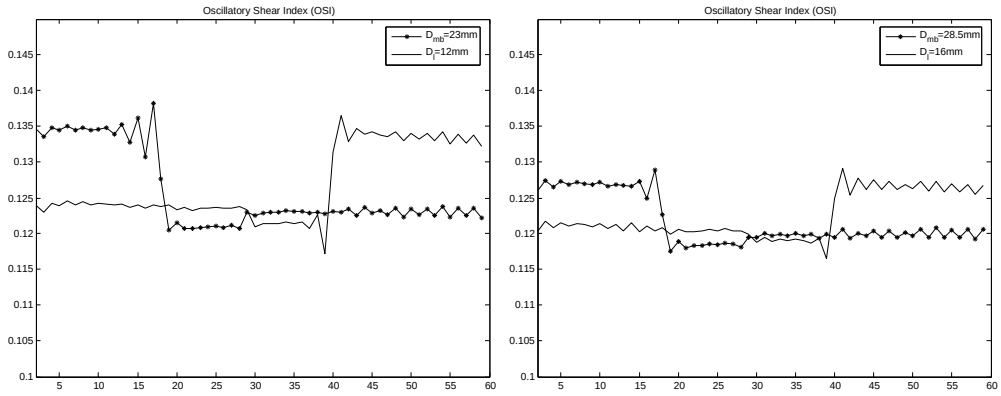

Fig. 4. Oscillatory Shear Index for rigid stent-graft with limb diameter equal to 12 mm and main body diameter 23 mm (left) and with limb diameter equal to 16 mm and main body diameter 28.5 mm (right)

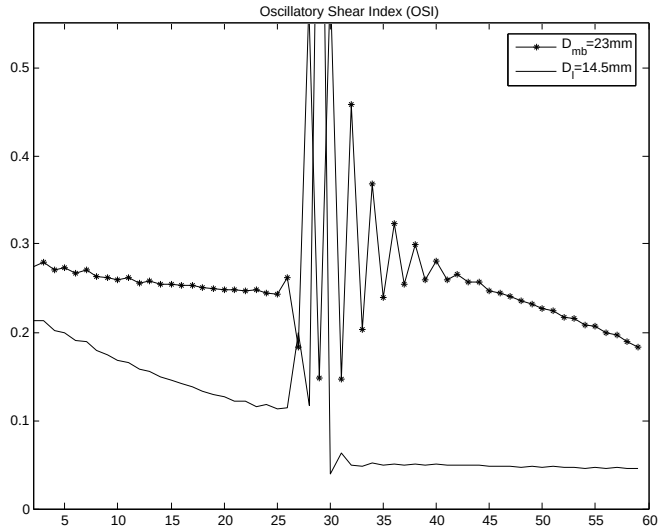

Fig. 5. Oscillatory Shear Index for compliant stent with limb diameter equal to 14.5 mm and main body diameter 23 mm

First, we present the results of the numerically computed OSI for two different prostheses flexibility parameters and different diameters of "parent" (main body) and "daughter" (limb) components.

On each of the Fig. 4, 5 the solid curve shows the Oscillatory Shear Index for the main body component from the anchoring site to the bifurcation point and the "solid-star" curve presents the OSI corresponding to the limb component from the bifurcation point downstream to the distal anchoring site.The Young's modulus of the prostheses shown in Fig. 4 corresponds to the one of rigid stent-graft, the main body diameters are 23 mm and 28.5 mm and the limb diameters are 12 mm and 16 mm. We observed that the smaller the diameter of the prosthesis the higher the OSI. We also tested a flexible prosthesis with a Young's modulus $E_c = 8700$ Pa (Fig. 5). The diameter of the main body for this case was taken to be 20 mm and the limb diameter is 14.5 mm. The

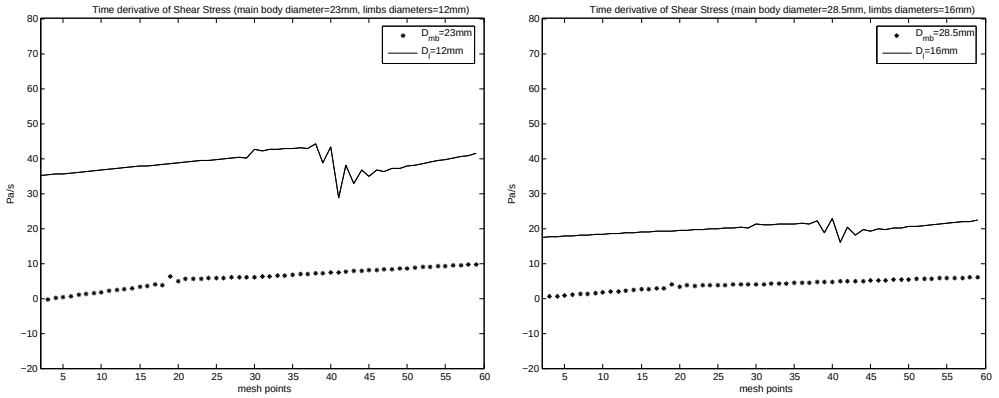

Fig. 6. Shear Stress Rates for rigid stent-graft with limb diameter equal to 12 mm and main body diameter 23 mm (left) and with limb diameter equal to 16 mm and main body diameter 28.5 mm (right)

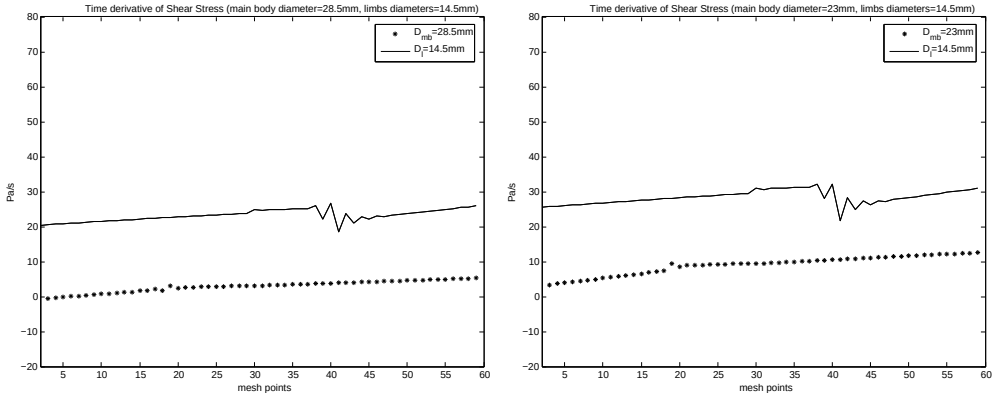

Fig. 7. Shear Stress Rates for the rigid stent-graft with a limb diameter equal to 14.5 mm and a main body diameter 28.5 mm (left) and with a limb diameter equal to 14.5 mm and a main body diameter 23 mm (right)

amplitude of the Oscillatory Shear Index drastically increased for this case, indicating a much higher probability for occlusion.

Although the OSI showed that the smaller the diameter of the limbs the higher the OSI, it did not capture the patient-observed prosthesis characteristics that show higher probability for thrombosis at the distal site and not typically at the proximal site of the prosthesis. In contrast, the shear stress rate of the bifurcated prostheses did show to be higher at the distal anchoring site thereby conforming better to the complications observed in patients.

Fig. 6–9 present the temporal gradient of shear stress at the systolic peak for different prostheses data. Again, each figure has two curves: solid curve corresponds to the shear stress rate of the main body component and "star" curve shows shear stress rate along the limb.

Fig. 6 shows the shear stress rates corresponding to the two extreme cases for compliant prosthesis: the prosthesis with the smallest limb diameter (12 mm) and the prosthesis with the largest limb diameter (16 mm), respectively. We observe that the smaller

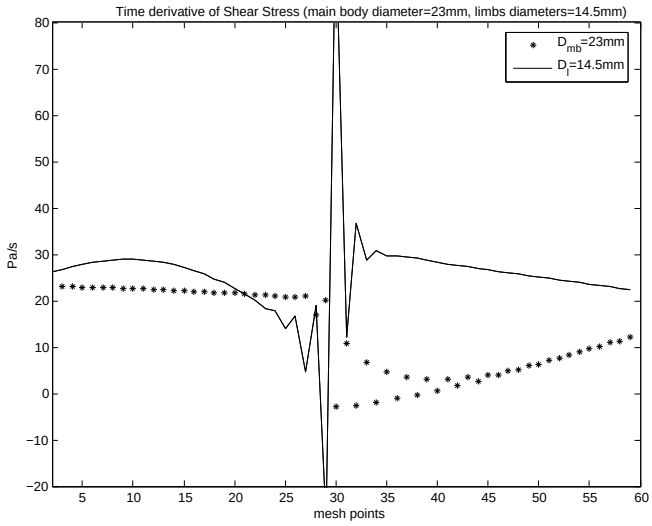

Fig. 8. Shear Stress Rates for the compliant endoprosthesis with a limb diameter equal to 14.5 mm and a main body diameter of 23 mm

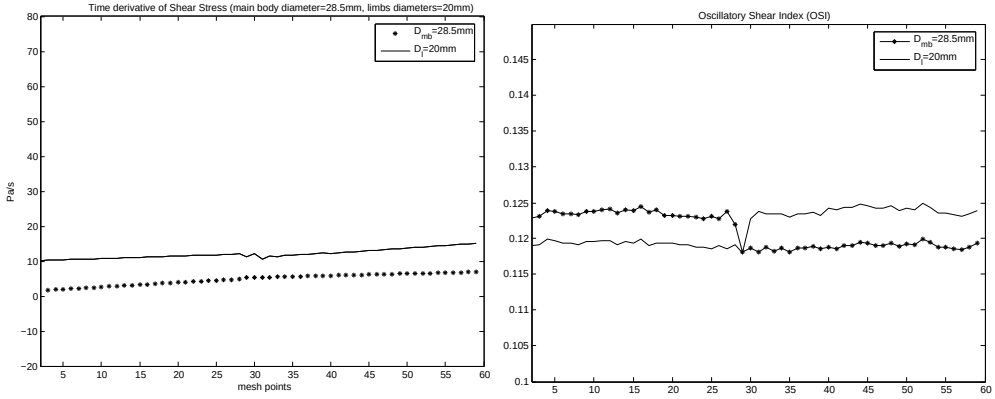

Fig. 9. Shear Stress Rates (left) and Oscillatory Shear Index (right) for an "optimal" stent with a limb diameter equal to 20 mm and a main body diameter of 28.5 mm

the diameter of the limbs the larger the shear stress rate, indicating a higher chance for occlusion. The worst performance was obtained for the smallest prostheses (Fig. 6 (left)) and the best performance was for prostheses with a limb diameter equal to 16 mm (Fig. 6 (right)).

We also observed that the size of the diameter of the main body influences the magnitude of the shear stress rate. Fig. 7 shows the comparison between two prostheses with the same limb diameters, but with different sizes for the main body: one with a main body diameter of 23 mm and the second one with a main body diameter of 28.5 mm. We can see an improvement in the shear stress rates for the larger main body prosthesis.

We calculated the shear stress rates for a bifurcated prosthesis with a compliancy $E_c = 8700$ Pa. As in the previous experiments for the "stiff" stent, we assumed that the diameter of the main modular component ranged from 23 mm to 28.5 mm, and that

the limbs diameter is between 12 mm and 16 mm. Fig. 8 presents the results of the numerical computations which indicate that the shear stress rates are drastically higher then for the case of stiff prosthesis.

The results presented above indicate that the magnitude of the shear stress rate is affected mainly by the size of the limbs and by the prostheses elasticity. In an attempt to obtain an optimal design minimizing shear stress rates we tested different prosthesis structures varying the limb diameter and elasticity parameters. We have found that the shear stress rate is minimized for the prosthesis with the following two characteristic:

- The diameter of the prosthesis limbs should be around $\sqrt{2}/2$ of the diameter of the main body component: if D_{mb} denotes the diameter of the main body component and D_l denotes the diameter of the limb component, then we obtained numerically that the lowest shear stress rates in the limbs are observed when $D_l = \frac{\sqrt{2}}{2} D_{mb}$. This relationship is a consequence of the conservation of mass principle.

- Variable elasticity: The prosthesis which is stiffer in the central section, where there is no support to the prosthesis walls by the walls of native aorta, and softer at the overlap with the iliac arteries, showed best performance. In this test we used the fact that the stiffness of the composit prosthesis/vessel structure is equal to the combined stiffness of each structure, [20]. Hence, the smaller the stiffness of the prosthesis in the overlap anchoring region, the smaller the difference between the stiffness of the native vessel and prosthesis.

Fig. 9 (left) shows the behavior of the shear stress rates for the "optimal" prosthesis with characteristics obtained from the suggestions above:

- Young's modulus in the overlap region $E_{overlap} = 8700$ Pa,

- Young's modulus of the prosthesis in the aneurysm sac region is equal to 100000 Pa,

- diameter of the main body component is $D_{mb} = 28.5$ mm,

- diameter of the limbs is $D_l = 20$ mm (which is about $\frac{\sqrt{2}}{2} D_{mb}$).

We observed a drastic improvement in the limb shear stress rates with respect to the previous prosthesis structures.

We also calculated the Oscillatory Shear Index for the "optimal prosthesis" described above (see Fig. 9 (right)). The results also showed a much smaller amplitude of OSI compared to the cases given in Fig. (4), (5).

Резюме

С.А. Лапин, С. Чанич. Численное моделирование дизайна раздваивающихся протезов используемых в лечении аневризмы брюшной аорты.

В статье рассматривается численное решение задачи взаимодействия крови со стенками артерий. Используется одномерная эффективная модель полученная асимптотически из уравнений Навье – Стокса для течения крови и уравнения линейной эластичной мембраны описывающего поведение стенок артерий. В этой работе рассматривается случай раздваивающихся эластичных артерий со вставленным протезом. Построенная модель используется для определения влияния касательного напряжения на появление и развитие атерогенеза.

Literature

1. *Čanić S., Krajcer Z., Lapin S.* Design of Optimal Endoprosthesis Using Mathematical Modeling // Endovascular Today. – 2006. – May. – P. 48–50 (Cover story).
2. *Nichols W.W., O'Rourke M.F.* McDonald's Blood Flow in Arteries: Theoretical, experimental and clinical principles. – N. Y., London, Sydney, Auckland: Arnold and Oxford University Press Inc., 1998.
3. *Wang R., Ravi-Chandar K.* Mechanical response of a metallic aortic stent-I. Pressure-diameter relationship // J. Appl. Mech. – 2004. – V. 71. – P. 697–705.
4. *Wang R., Ravi-Chandar K.* Mechanical response of a metallic aortic stent-II. A beam on elastic foundation model // J. Appl. Mech. – 2004 – V. 71. – P. 706–712.
5. *Umscheid T., Stelter W.J.* Time-related alterations in shape, position, and structure of self-expanding, modular aortic stent-grafts // J. Endovasc. Surg. – 1999. – V. 6 – P. 17–32.
6. *Čanić S., Hartley C.J., Rosenstrauch D., Tambača J., Guidoboni G., Mikelic A.* Blood flow in compliant arteries: an effective viscoelastic reduced model, numerics and experimental validation // Ann. Biomed. Eng. – 2006. – V. 34. – P. 575–592.
7. *Čanić S., Mikelic S.A., Lamponi D., Tambača J.* Self-consistent effective equations modeling blood flow in medium-to-large compliant arteries // SIAM J. Multiscale Analysis and Simulation. – 2005 – V. 3, No 3. – P. 559–596.
8. *Čanić S., Kim E.H.* Mathematical analysis of the quasilinear effects in a hyperbolic model of blood flow through compliant axisymmetric vessels // Math. Methods in Appl. Sciences. – 2003. – V. 26. – P. 1161–1186.
9. *White F.M.* Viscous Fluid Flow. – N. Y.: McGraw-Hill, 1974.
10. *Smith N.P., Pullan A.J., Hunter P.J.* The generation of an anatomically accurate geometric coronary model // Ann. Biomed. Eng. – 2000. – V. 28, No 1. – P. 14–25.
11. *Smith N.P., Pullan A.J., Hunter P.J.* An anatomically based model of transient coronary blood flow in the heart // SIAM J. Appl. Math. – 2002. – V. 62. – P. 990–1018.
12. *Olufsen M., Peskin C., Kim W., Pedersen E., Nadim A., Larsen J.* Numerical simulation and experimental validation of blood flow in arteries with structured-tree outflow conditions // Ann. Biomed. Eng. – 2000. – V. 28. – P. 1281–1299.
13. *Marusic-Paloka E.* Fluid flow through a network of thin pipes // Comptes Rendus de l'Academie des Sciences Paris, Serie II, Fascicule B – Mecanique. – 2001. – V. 329, No 2. – P. 103–108.
14. *Smoller J.* Shock waves and reaction-diffusion equations. – N. Y.: Springer-Verlag, 1994.
15. *Leveque R.* Numerical Methods for Conservation Laws. – Basel; Boston: Birkhäuser, 1992.
16. *Parent F.N., Godziachvilli V., Meier G.H., Parker F.M., Carter K., Gayle R.G., Demassi R.J., Gregory R.T.* Endograft limb occlusion and stenosis after ANCURE endovascular abdominal aneurysm repair // J. of Vasc. Surg. – 2002. – V. 35, No 4. – P. 686–690.
17. *Ku D.N., Giddens D.P., Zarins C.K., Glagov S.* Pulsatile flow and atherosclerosis in the human carotid bifurcation: positive correlation between plaque location and low and oscillating shear stress // Atherosclerosis. – 1985. – V. 5. – P. 293–302.
18. *Moore J.E., Xu C., Glagov S., Zarins C.K., Ku D.N.* Fluid wall shear stress measurements in a model of the human abdominal aorta: oscillatory behavior and relationship to atherosclerosis // Atherosclerosis. – 1994. – V. 110. – P. 225–240.

19. *Haidekker M.A., White C.R., Frangos J.A.* Analysis of temporal shear stress gradients during the onset phase of flow over a backward-facing step // J. Biomech. Eng. – 2001. – V. 123, No 5. – P. 455–463.

20. *Dyet J.F., Watts W.G., Ettles D.E., Nicholson A.A.* Mechanical properties of metallic stents: How do these properties influence the choice of stent for specific leisons? // Cardiovasc. Interv. Radiology. – 2000. – V. 23. – P. 47–54.

Поступила в редакцию
15.08.06

Лапин Сергей Александрович – ассистент Департамента математики Университета Хьюстона, г. Хьюстон, США.

E-mail: *slapin@math.uh.edu*

Чанич Сунчица – профессор Департамента математики Университета Хьюстона, г. Хьюстон, США.

E-mail: *canic@math.uh.edu*